PCCP

Accepted Manuscript

ROYAL SOCIETY OF CHEMISTRY

www.rsc.org/pccp

Electronic structure dynamics in a low bandgap polymer studied by time-resolved photoelectron spectroscopy

Ute B. Cappel,[1,b*] Stefan Plogmaker,[1,b] Joachim A. Terschlüsen,[1] Torsten Leitner,[1,2] Erik M. J. Johansson,[3] Tomas Edvinsson,[4] Anders Sandell,[1] Olof Karis,[1] Hans Siegbahn,[1] Svante Svensson,[1,2] Nils Mårtensson,[1,2] Håkan Rensmo,[1] Johan Söderström[1]

1 Division of Molecular and Condensed Matter Physics, Department of Physics and Astronomy, Uppsala University, Box 516, 751 20 Uppsala, Sweden

2 Uppsala-Berlin joint Laboratory on next generation photoelectron spectroscopy, Albert-Einstein-Str. 15, 12489 Berlin, Germany

3 Department of Chemistry - Ångström Laboratory, Uppsala University, Box 523, 751 20 Uppsala, Sweden

4 Department of Engineering Sciences – Solid State Physics, Uppsala University, Box 534, 751 21 Uppsala, Sweden

b These authors contributed equally to this work.

* Ute.cappel@physics.uu.se

Abstract

Means to measure the temporal evolution following a photo-excitation in conjugated polymers are a key for the understanding and optimization of their function in applications such as organic solar cells. In this paper we study the electronic structure dynamics by direct pump-probe measurements of the excited electrons in such materials. Specifically, we carried out a time-resolved photoelectron spectroscopy (TRPES) study of the polymer PCPDTBT by combining an extreme ultraviolet (XUV) high harmonic generation source with a time-of-flight spectrometer. After excitation to either the 1st excited state or to a higher excited state, we follow how the electronic structure develops and relaxes on the electron binding energy scale. Specifically, we follow a less than 50 fs relaxation of the higher exited state and a 10 times slower relaxation of the 1st excited. We corroborate the results using DFT calculations. Our study demonstrates the power of TRPES for studying photo-excited electron energetics and dynamics of solar cell materials.

Introduction

Knowledge-based development of organic photovoltaics critically depends on gaining understanding of the mechanism of the electronic structure dynamics, the charge separation processes within the active layer and on determining energetic losses within the solar cell. This includes the absorption process, the fate of the primary photo-excitations such as vibrational relaxation and internal conversion as well as the charge separation. The main steps in these processes are now generally accepted to be as follows:[1] After light absorption and subsequent relaxation excitons are formed in a p-type organic semiconductor and diffuse to an interface with the electron acceptor

(typically derivative of C_{60}). Here they can be split into separate charges in order for the solar cell to generate current. Charge separation at the donor/acceptor interface often involves the formation of bound charge transfer states and a significant energetic loss.[2] As typical exciton diffusion lengths are often in the order of only tens of nanometers, a bulk heterojunction architecture is usually employed: the donor and acceptor are mixed in the active layer of the solar cell and a large interface area between the two materials is achieved.[3,4] Femtosecond transient absorption spectroscopy has often been the tool of choice for determining the details of the dynamics involved in the charge generation mechanism.[5,6] However, the interpretation of the data can be significantly complicated by the overlap of spectral signals such as those arising from excitons, charge-transfer states or free polarons and the energies of the excited and transient states are not directly measured.

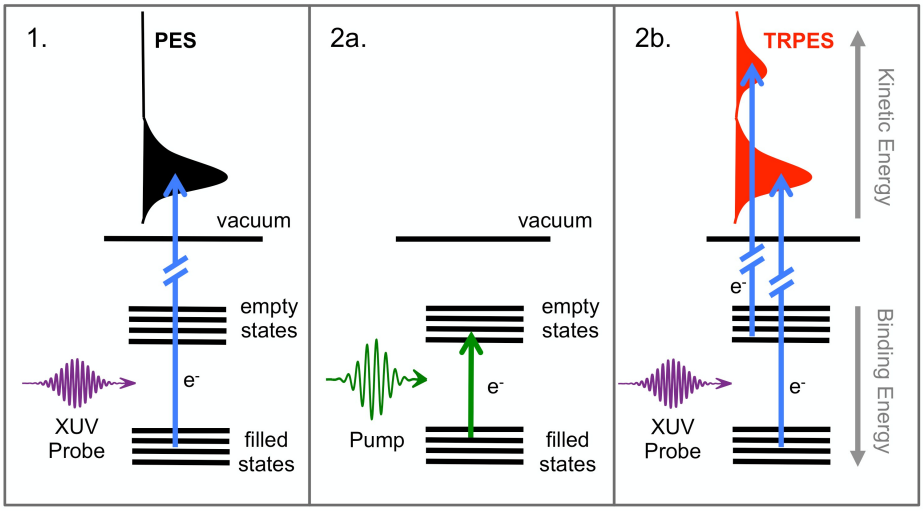

Figure 1 Schematic diagram of the concepts behind time-resolved photoelectron spectroscopy. 1. Photoelectron spectroscopy: The XUV pulse is used to emit electrons from a material and the kinetic energies of the electrons are measured. 2. Time resolved photoelectron spectroscopy: a. The pump pulse is used to excite electrons from filled to empty states. b. The XUV probe is used to emit electrons from the ground state and from the excited state. The kinetic energy of the emitted electrons is measured. Changing the delay between the pump and XUV probe pulse results in a time-resolved photoelectron spectra.

Extreme ultraviolet (XUV) based time-resolved photoelectron spectroscopy (TRPES) can be used to directly measure the excited electronic structure of materials together with its evolution over time. In this technique, just like in many other time-resolved spectroscopies, a laser pump pulse is used to bring a material into an excited state and a second light pulse is used to probe the excited state (Fig. 1). However, instead of probing the excited state by measuring the absorption of the probe pulse as in transient absorption spectroscopy, a XUV probe pulse with photon energy sufficient to emit photoelectrons from the material over a broad range (from core levels up to valence levels) is used. By measuring the kinetic energies of the emitted electrons, the initially occupied states and the electronic states populated by the photoexcitation process can be probed simultaneously and in an identical way. The technique is selective to electronic states close to the sample surface due to the short mean free path of electrons in solids.

Femtosecond time resolution in TRPES measurements can be achieved through the use of high power femtosecond lasers, which can be used to generate the pump and probe pulses.[7–12] So far such measurements have been mainly carried out with both the pump and probe energies in the near infrared to UV regimes (up to ~6 eV). In this case, only electrons, which have interacted with photons from both pulses, will be emitted from the sample and the technique is then often referred to as (time resolved) two-photon photoemission spectroscopy (2PPE).[10–12]

In contrast, the use of XUV probe pulses, which can be obtained in a high harmonic generation (HHG) process,[13] allows for the simultaneous measurement of both the occupied (including core levels potentially allowing for element specific studies) and the initially unoccupied photoexcited states on a common energy scale (Fig. 1). With this technique one can follow in detail how the photoexcited state evolves with time after the photoexcitation. One can for instance directly see if the excited state depopulates via transitions to intermediate states.

However, the application of TRPES to the study of the dynamics and energetics of organic solar cell materials is highly challenging. One has to detect very small changes in the electronic structure while using low intensities for both the pump and the probe. The pump should only bring a small fraction of the valence electrons into the excited states for the measurement to be relevant for solar cells. The low probe intensity is needed to minimize radiation damage of the organic materials. Furthermore, one may need to reduce the probe intensity in order to avoid broadenings of the spectra due to space-charge effects (Coulomb repulsion between all the emitted electrons). This problem is particularly visible for very short probe pulses, as these leads to high peak intensities. Finally, it is also important to reduce the measurement times for the individual spectra as much as possible in order to be able to measure spectra at many different pump-probe delays within a reasonable time. All these demands call for a highly efficient spectrometer set-up.

In this work, we show that these challenges can be overcome by combining an HHG source[14,15] with an angle resolved time-of-flight (ARTOF) spectrometer for TRPES measurements. The ARTOF spectrometer[16] has a very high electron collection efficiency as it analyzes a wide cone of emitted electrons simultaneously. It is based on an advanced electron lens system. A position sensitive detector records the flight time and the hit position on the detector for each electron emitted within the acceptance cone of the spectrometer. This information can be uniquely transformed to the angle of emission and the kinetic energy of the photoelectron. Since each flight path within the lens system is treated separately this implies that a very high energy resolution can be obtained for this time-of-flight set-up compared to other types of time-of-flight spectrometers. In comparison to state-of-the-art hemispherical electron spectrometers the ARTOF spectrometer allows for an increase in obtainable information rate by two to three orders of magnitude. Such an instrument is therefore ideally suited for spectroscopic studies of radiation sensitive samples since a much lower XUV fluence can be used. The high sensitivity makes it also possible to monitor low fractions of excited electrons.

In the following, we demonstrate that the combination of an HHG source and an ARTOF spectrometer can be used to measure TRPES of organic solar cell materials by showing the example of the polymer PCPDTBT (poly[2,6-(4,4-bis-(2-ethylhexyl)-

4*H*-cyclopenta [2,1-*b*;3,4-*b*′]dithiophene)-*alt*-4,7(2,1,3-benzothiadiazole)]). PCPDTBT (Fig. 2a) is a low band gap polymer which has given high efficiencies in bulk-hetero junction solar cells[17,18] and has been the focus of many mechanistic studies.[19–24] With support from density functional theory (DFT) calculations, the TRPES method gives insights into the energetics of electrons in the polymer's excited states and on the dynamics of relaxation processes.

Experimental methods

PCPDTBT (1-Material) was deposited on an ITO substrate by spin-coating at 1000 rpm from a 5 mg/ml chlorobenzene solution for all measurements. The absorption of the sample was measured using an HR-2000 Ocean Optics fiber optics spectrophotometer.

Time-resolved photoelectron spectroscopy was performed at the surface science beamline of the HELIOS light source at Uppsala University.[14,15] The sample was excited by weakly focused 400 nm / 800 nm (1.0 mm / 0.7 mm FWHM) pulses with an intensity of 700 / 270 nJ (89 / 70 μJ cm^{-2}). The pulse length of the 800 nm pulses was measured with an optical autocorrelator (APE pulseCheck) to be 35 fs FWHM whereas the pulse length of the 400 nm radiation was extracted from the experimental data and found to be approximately 110 fs.

The XUV probe pulses were generated by focusing 0.2 mJ of the 800 nm Ti:sapphire driving laser into a 16 mm long gas cell that was mounted inside a vacuum chamber. The cell was flooded with argon gas with a pressure of 83 mbar. In the interaction of the driving laser with the argon gas a wide band of harmonics is generated and co-propagates with the residual laser beam into an XUV monochromator. The residual 800 nm laser is reflected out of the XUV beam path by a 200 nm thick aluminum foil mounted in the entrance of the monochromator. The monochromator was set to transmit the 25th harmonic (~39 eV) and a bandwidth of 150 meV was selected. The XUV pulse length at this monochromator setting was determined to be typically about 38 fs FWHM. The XUV radiation is subsequently focused down to 0.15 mm diameter onto the sample where it is spatially overlapped with the pump beam.
The arrival time at the sample of the pump pulse relative to the probe pulse can be varied by a motorized delay stage (Aerotech L-ANT130-160-L). To determine the time zero and the full width at half maximum (FWHM) of the cross correlation of the probe and the 800 nm pump at the sample, side bands were measured on helium gas.[14] For the 400 nm pump, we were not able to measure side bands due to the lowered intensity of the pump beam at this wavelength. Instead, we determined time zero and FWHM from the measurements on PCPDTBT. The kinetic energy of the ejected electrons in the sideband measurements as well as the measurements on PCPDTBT were analyzed by a Scienta ARTOF 10k prototype electron spectrometer.[16] The angular resolution of this spectrometer was not of importance for these measurements and was not considered in the data analysis.

As the ARTOF is only capable of analyzing one electron per laser shot, the count rate in the ARTOF was kept below the repetition rate of the laser by adjusting the XUV fluence at the sample through reducing the size of the exit slit of the monochromator.
The laser was operated at a repetition rate of 10 kHz. Spectra of PCPDTBT were acquired at 16 delay stage positions for one minute (600,000 laser shots) each. The delay stage was then moved back to the original position and the process was

repeated. During the first 30 minutes of measurement a minor shift in the spectrum was observed, which did not affect the observation of signal from the excited state(s). Following this, the signal observed for both ground and excited state electrons was stable for several hours before the signal began to decrease. We used the time region where the spectra were not changing to obtain the spectra and time traces shown in this paper by averaging 11 one minute spectra at each delay stage position. Measurements with 800 and 400 nm were carried out on fresh spots of the sample explaining a small variation between the shapes of the HOMO peaks. In order to have an internal reference system in binding energy, 0 eV binding energy was fixed to the HOMO onset in the PCPDTBT spectra where the XUV pulse arrived at the sample before the pump pulse as shown in Fig. 2b. Comparing to reference 25, the Fermi level is estimated to be at about -0.3 eV.
The least square fitting of kinetic traces was carried out in IGOR Pro (Wavemetrics) using the built-in curve fitting capabilities.

Density functional theory (DFT) calculations were performed using the Gaussian 09 quantum chemical package.[26] The geometries were optimized on the B3LYP/6-311G(d,p) and B3LYP/6-311+G(d,p) level, as these have been shown to give good agreements of optical band gaps with experimental data.[27,28] Time-dependent DFT was utilized to calculate the vertical transition probabilities to obtain the theoretical UV-visible spectra and optically active states.

Results and Discussions

Figure 2b shows a regular valence spectrum of the PCPDTBT polymer film measured using the TRPES set-up with the 25th harmonic (~39 eV) generated in argon gas. The pump pulse was blocked for this measurement. The spectrum shows a broad peak, which contains contributions from several levels according to DFT calculations on oligomers (monomers to pentamers) of the CPDTBT unit (Table S1). The spectrum also shows a tail-like distribution of states at low binding energies, which can be attributed to defects and disorder in the polymer structure.[29,30] In order to facilitate the discussion of the time-resolved data, we refer all binding energies in our spectra to the onset of occupied states as shown in Fig. 2b. We also characterized this film by core level photoelectron spectroscopy (see Supporting Information). Our core and valence level results match well with previously reported spectra for PCPDTBT[25] and demonstrate that we have high quality films of the polymer.

The UV-visible absorption spectrum of the polymer film is shown in Fig. 2c. The spectrum shows a broad absorption between approximately 550 and 850 nm with a maximum at 780 nm. A second higher energy absorption feature is observed with a peak at approximately 430 nm. The peak at 780 nm has previously been assigned to the transition from the highest occupied molecular orbital (HOMO) to the lowest unoccupied molecular orbital (LUMO) and shows a vibronic replica at 700 nm.[19,31] We compared our absorption spectrum to theoretical absorption spectra of the CPDTBT oligomers without alkyl groups calculated with TD-DFT at a B3LYP/6-311G(d,p) level and found that the experimental absorption properties of the polymer film are matched best by the optical behavior of the calculated trimer (Fig. 2c and Tables S2-S4). The excitation wavelengths used in TRPES are indicated in Fig. 2c as solid colored bars, namely the fundamental of a Ti:sapphire laser at 800 nm and the frequency doubled radiation at 400 nm.

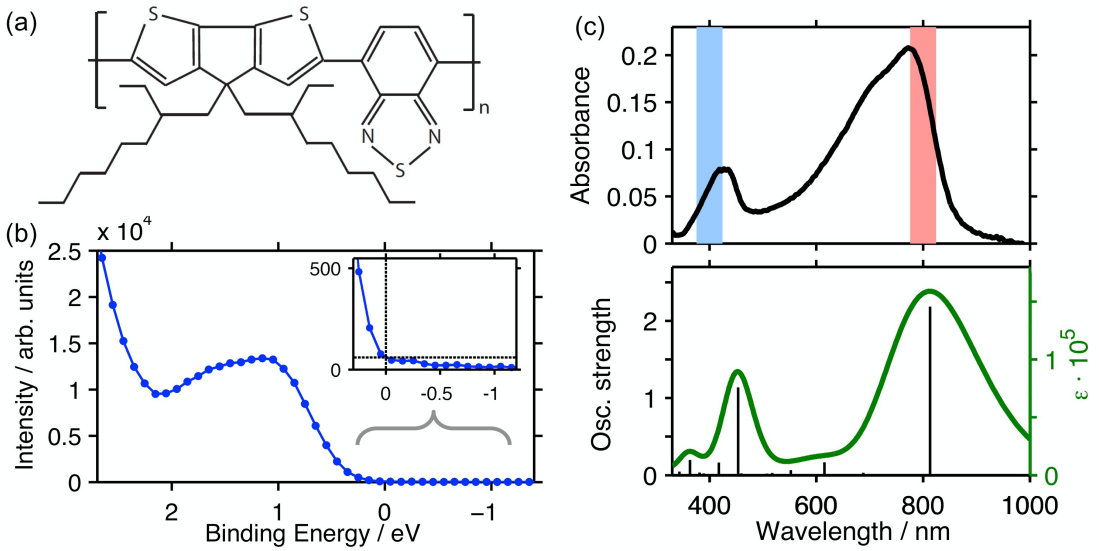

Figure 2 Steady-state properties of PCPDTBT. a) Molecular Structure of PCPDTBT, b) Valence photoelectron spectrum of PCPDTBT on ITO measured with the HHG source and the ARTOF spectrometer. The inset shows the onset of occupied states set to 0 eV binding energy. c) Top: Absorption spectrum of PCPDTBT film on ITO with the TRPES pump wavelengths of 400 and 800 nm indicated, Bottom: Absorption spectrum of CPDTBT trimer calculated with TD-DFT with the oscillator strengths of the individual transitions shown on the left axis and the extinction coefficient ε on the right axis.

Figure 3 shows the pump-probe photoelectron spectra of PCPDTBT using both the XUV probe pulse and either the 800 nm or the 400 nm pump pulse. The relative arrival times of the pump and probe at the sample were varied by means of a delay stage. Figure 3a,b shows photoelectron spectra where the XUV probe arrived at the sample 150 fs before the pump pulse (-150 fs) and 30 fs after it (+30 fs) for pump wavelengths of 800 and 400 nm. When the probe arrives at the sample after the pump, small photoemission structures are detected in addition to those arising from the ground state for both excitation wavelengths. Following the representation in Fig. 1, these features stem from photoemission of electrons from initially unoccupied, photoexcited states of PCPDTBT and will be referred to as excited electrons in this paper. In general, their binding energies are negative with our definition of the binding energy scale. When pumping with 800 nm, the signal of excited electrons gives rise to a peak at approximately -0.5 eV. With a pump wavelength of 400 nm, a clear peak is absent but electrons are observed further away from the valence band onset (at lower binding energies) than for 800 nm excitation (to about -2 eV). The intensity of the excited electron structure is more than 100 times smaller than the valence structure intensity of the ground state for both excitation wavelengths strongly suggesting that only a small fraction of valence electrons has been excited. This clearly demonstrates that our set-up with a high transmission ARTOF spectrometer allows for the detection of a low concentration of excited electrons. We note that we do not observe a significant decrease in the magnitude of the HOMO peak, as a relative variation of less than 1% in the signal intensity is not detectable given the signal-to-noise in the measurement at these energies. In the further analysis of the spectra, we therefore solely focus on the region where we observe excited electrons.

Figure 3c,d shows selected spectra at different delay times overlaid with a spectrum measured at a delay time of -1000 fs (corresponding to the signature of the ground state) for pump wavelengths of 800 nm (Fig. 3c) and 400 nm (Fig. 3d). In both cases, clear signals of excited electrons are observed at time zero and at positive delay times. When exciting with 800 nm, excited electrons are observed down to binding energies of -1 eV for all positive delay times. The intensity of the excited electrons decreases over time and also the distribution shifts to binding energies close to the valence band onset at 0 eV. These spectra highlight the strength of the technique in terms of following how the electron binding energies in the excited state develop with time in relation to the energies in the ground state.
When exciting with 400 nm, electrons are observed down to binding energies of -2 eV at delay times close to time zero, while as the delay time increases they are mostly observed at binding energies larger than -1 eV. At delay times of a few hundred femtoseconds and longer, the spectra observed with 400 nm excitation become very similar to those observed with 800 nm excitation and the same shift to binding energies close to the valence band onset at 0 eV is observed. This suggests that the electrons populate the same states for both excitation wavelengths at these delay times.

None of the spectra display a clear dip in the spectral intensity that can be associated with a traditional band gap region. A band gap region would be expected from traditional representations of a crystalline semiconductor, where electronic states are nearly absent in between the valence and conduction bands. However, PCPDTBT has an amorphous structure and as described above, its absorption properties are well matched with calculations of a CPDTBT trimer (Fig. 2d). This matching suggests that the effective conjugation length in the polymer film is perturbed and the optical transitions in the polymer can be modeled by an effective conjugation length of approximately a trimer. It therefore seems appropriate to describe the results using a molecular picture and we will discuss our results in terms of the molecular orbitals and electronic transitions calculated for the trimer (Fig. 4a). The trimer calculations show a feature at 813 nm with contributions mainly from a HOMO to LUMO transition. The higher energy absorption (418 nm) feature in the trimer is a combination of many transitions with the major contribution (93%) from a HOMO to LUMO+3 transition (see Tables S3 and S4). The trimer's LUMO+3 has a higher electron localization on the thiophene units than the LUMO (Fig. 4a,b). With these theoretical findings in mind and in agreement with other DFT calculations of PCPDBT,[19,31] we will in the remainder of this paper refer to the excited state formed with 800 nm excitation as S_1 and to the excited state formed with 400 nm excitation as S_n. Moreover, excitation of electrons with 800 nm forming the S_1 state can, according to the calculations, largely be described as a HOMO to LUMO transition in a one electron picture.

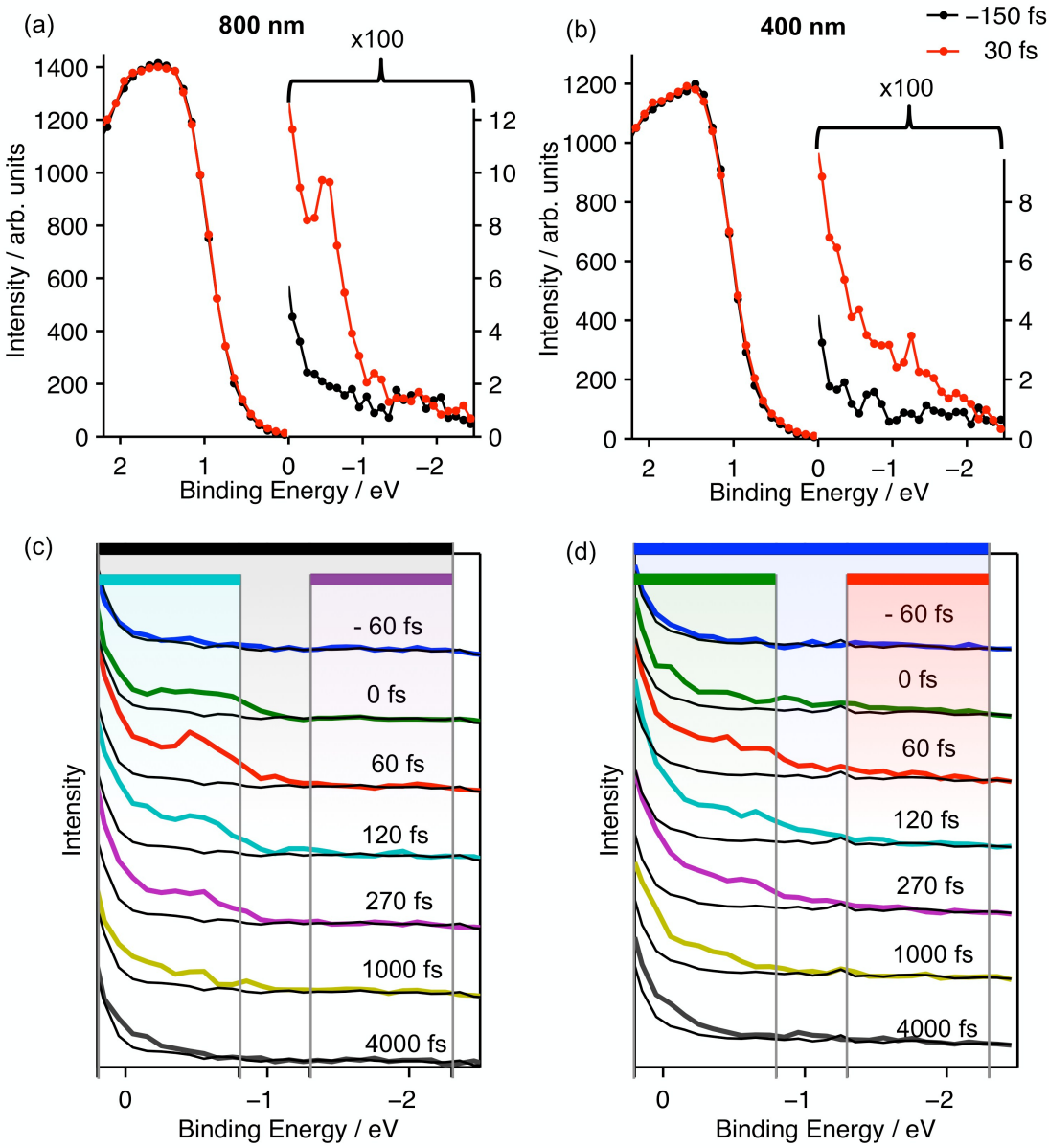

Figure 3. Time-resolved photoelectron spectra of PCPDTBT. a,b) With the probe arriving 150 fs before the pump (black) and 30 fs after the pump (red) measured with a pump of 800 nm (1.55 eV, a) and measured with a pump of 400 nm (3.1 eV, b). c,d) Spectra at selected pump probe delay times offset and overlaid with a spectrum measured at -1000 fs excited with 800 nm (c) and 400 nm (d). The energy regions for the integration of electron counts are indicated in the same colors as used in Fig. 5 when displaying the resulting kinetic traces.

As described above, the electrons in PCPDTBT exhibit an energy distribution due to different molecular orientations and different surroundings of the polymer chains in the sample, leading to the observation of a broad peak in the ground state and a significant number of tail states (Fig. 2b). Excitation of electrons from the HOMO to the LUMO with 800 nm forming the S_1 state correspondingly leads to a distribution of electron binding energies in the S_1 excited state with a maximum at -0.5 eV binding energy. A schematic diagram of this molecular one electron picture is shown in Fig. 4c: excitations at individual sites require photons with the energy of the

bandgap or higher, but a distribution of the ground state binding energies for different sites leads to an equally broad energy distribution of the energies of excited electrons. For a sufficiently broad distribution in such a system, no bandgap region is observed. From the position of the excited electron peak (-0.5 eV) and the photon energy (1.55 eV) we can conclude that the excitations do not simply originate from the onset of the valence electron distribution as would be expected in a standard semiconductor view for excitations close to the bandgap energy. This suggests that a molecular, disordered picture of the system is more appropriate here and that we can discuss excitations with 800 nm in terms of local excitations to the S_1 state. At negative delay times and at short positive delay times before nuclear relaxation can occur, the polymer will be in a nuclear configuration of its ground state throughout the photoemission process. For measurements at longer delay times, the nuclei have time to respond to the new electronic environment. We therefore assign the shift in the excited electronic distribution occurring from 60 fs to 4 ps to the vibrational relaxation of the nuclei to the relaxed geometry for the first singlet excited state.

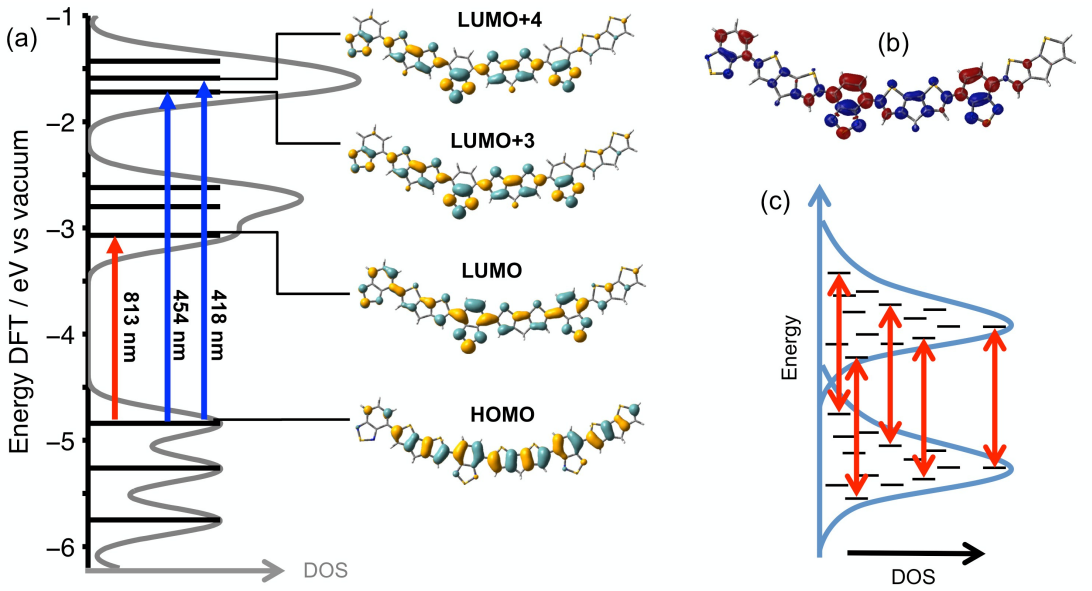

Figure 4 a) Density of states predicted for the CPDTBT trimer using DFT calculations. The relevant transition lines for 400 nm and 800 nm excitation calculated using TD-DFT are indicated. b) Difference in electron density in LUMO and LUMO+3 calculated from the squared molecular orbital distributions. Red indicates more electron density in LUMO, blue more electron density in LUMO+3. c) Schematic representation of HOMO and LUMO distributions in a system where local states have different energies. The local states are indicated by horizontal black lines and the bandgap for each state is indicated by a red arrow.

Excitation with 400 nm should lead to the formation of the S_n excited state and we expect to observe excited electrons at binding energies approximately 1.5 eV more negative than those in the S_1 excited state (Fig 4a). While electrons are observed at such energies at delay times of 0 fs and 60 fs, electrons are also observed at binding energies assigned to the S_1 excited state. We used a simplified approach to estimate the time evolution of the intensities at different electron binding energies to compare the kinetics of the S_1 and S_n excited states over all delay times. We integrated the signal in each of three different binding energy regions (indicated in Fig. 3c and 3d)

to follow the overall kinetics of excited electrons as well as the kinetics of the electrons in the specific excited states. We chose a region from 0.2 to -2.3 eV to give a measure of the total number of excited electrons. For an estimate of the number of excited electrons associated with the S_1 and S_n excited states, we chose regions of 1 eV width at respective ends of the total energy distribution: The S_1 region from 0.2 to –0.8 eV and the S_n region from -1.3 to -2.3 eV. Using these regions ensures that most of the distributions representing S_1, observed for excitations with 800 nm, are represented in the first region. This approach is an approximation and may be influenced by some redistribution of intensities at binding energies associated with the S_1 an S_n states. We found that small changes in the chosen regions influenced the absolute counts in each region but not the trends, which are described below.

The resulting kinetic traces are shown in Fig. 5 (error analysis in Fig. S4 and S5). For 800 nm excitation, it can clearly be seen that electrons are only excited to the S_1 state and that, as expected, the S_n states are not populated (Fig. 5a). For excitation with 400 nm, still most signal falls within the energy range of the S_1 state (0.2 to -0.8 eV, Fig. 5b). However, a small, short-lived signal of S_n electrons (-1.3 to -2.3 eV) is observed (Fig. 5b). This signal has decayed to within the noise level at less than 200 fs delay time (Figure S5).

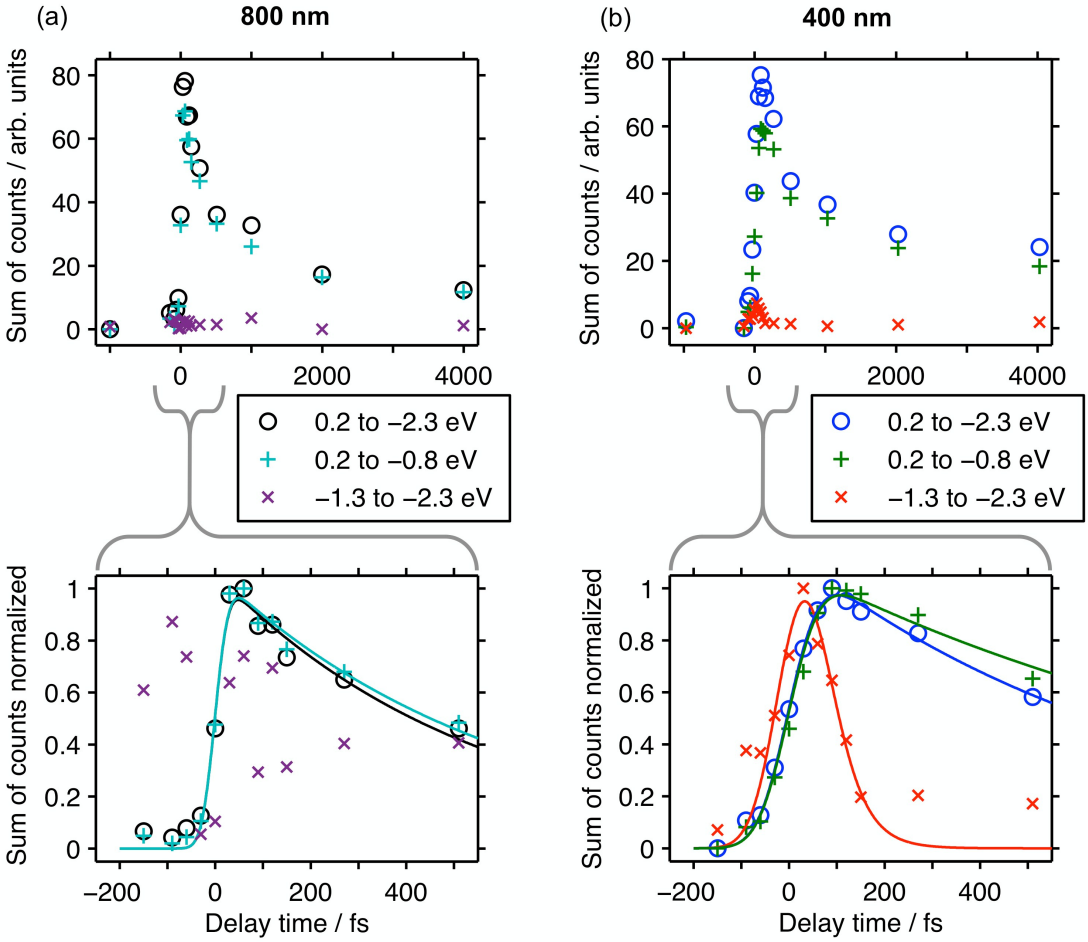

Figure 5 Kinetic traces following excitation at 800 nm (a) and 400 nm (b) obtained by summation of the counts in different regions of the single delay spectra (as shown in Figure 3). Traces in the top panels were baseline corrected by subtracting the minimum count value. The traces in bottom panels were scaled to values

between 0 and 1 and solid lines represent convoluted exponential fits to the data between -200 and 500 fs.

To quantify the time resolution of our set-up and compare the S_1 and S_n decay kinetics, we fitted the initial decay of the signal (up to 500 fs) with a single exponential convoluted with a Gaussian (see Supporting Information for details of the fitting procedure[32] and Fig. 5 and Table 1 for the resulting parameters). The values for time zero and the full width half maximum determined from sideband measurements were used in the fit of the 800 nm data, which reproduced the data well. For 400 nm, time zero and FWHM were determined by fitting the signal of all excited electrons (0.2 to -2.3 eV) and then fixed at the determined values for the fits of the other energy regions. A FWHM of 120 fs was obtained this way, which is longer than the FWHM at 800 nm due to a temporal broadening of the 400 nm pulse. At 800 nm, all excited electrons (0.2 to -2.3 eV) and the S_1 electrons (0.2 to -0.8 eV) show a very similar initial decay constant confirming that excitation to higher excited states is negligible at this low excitation energy. At 400 nm, different time constants are observed for the three regions (see Table 1). The signal from S_n electrons (-1.3 to -2.3 eV) decays quickly with a time constant shorter than 50 fs. Electrons remain in the S_1 state (0.2 to -0.8 eV) much longer as they have an initial decay time longer than 1 ps. The kinetics for all excited electrons should be the sum of the individual exponentials for the two decay pathways. However, given the limited amount of time points in our fit region, we also fitted this data with a single exponential. The fitted time constant for this region lies in between the time constants for the two separate regions.

Table 1. Fit constants with standard deviation of convoluted exponential fitting of the data in Figure 4b and d.

λ_{pump} / nm	Sum region / eV	Gaussian FWHM / fs	Exponential decay time τ / fs
800	0.2 to -2.3	52 (fixed)	550 ± 70
800	0.2 to -0.8	52 (fixed)	600 ± 60
400	0.2 to -2.3	120 ± 10	770 ± 60
400	0.2 to -0.8	120 (fixed)	1100 ± 100
400	-1.3 to -2.3	120 (fixed)	45 ± 10

The initial S_1 lifetimes observed here (600 fs for 800 nm and 1100 fs for 400 nm) appear short compared to exciton lifetimes of around 100 ps measured by transient absorption spectroscopy.[19,33] A clear difference between the two types of measurement consists in the depth of the sample being probed. While transient absorption spectroscopy probes the entire depths of the sample, our TRPES measurements only probe the sample surface region and we therefore study the behavior of excited states in this region only. Surface and interface kinetics are important for the charge transfer in solar cells and our measurements are therefore complementary to transient absorption spectroscopy. It has been shown that excited state lifetimes in conjugated polymers do not follow single exponential kinetics at high concentrations, which are generated during the short pump pulses in femtosecond spectroscopy.[33–35] In our present investigation, we can estimate the concentration of absorbed photons in the top 1 nm at the sample surface to be 0.04 photons/nm^3 (4 x 10^{19} photons/cm^3) for 800 nm and 0.008 photons/nm^3 (8 x 10^{18}

photons/cm^3) for 400 nm excitation (see Supporting Information). The light intensities should therefore be sufficiently low to prevent multiple excitations per site of the polymer, but are in a concentration regime in which exciton-exciton annihilation can occur (above concentrations of 10^{17} photons/cm^3).[35] There is therefore an interest to further push for lower detection limits thus lower possible pump intensities in future studies with TRPES.

Given that the fitted lifetime of electrons in the S_n excited state is shorter than the FWHM of the pulse convolution, it is clear that relaxation of the electrons in the S_n state occurs within the time window of the measurement. That is, the spectra recorded after excitation to the S_n state at a delay time of 0 fs will already have a contribution of the states after electronic relaxation in addition to the contribution of the initial excited state. The relative intensities of the different states will depend on the relation between the time resolution of the measurement and the lifetime of electrons in the S_n state. The spectra measured upon excitation with 400 nm exhibit only a minority of the excited electrons in the S_n state while the majority of the excited electrons occupy the S_1 state. From this follows that the fast decay of S_n electrons is predominantly due to a fast internal conversion process to the S_1 excited state. The larger population of the S_1 state is the result of having a time window of the measurement (120 fs) that is significantly longer than the S_n lifetime (< 50 fs). At longer delay times, electrons are only observed in the S_1 excited state and this leads to a strong similarity between the spectra recorded at 400 nm and 800 nm excitation, as noted above.

According to the DFT calculations, the $S_n \rightarrow S_1$ conversion might correlate with a decrease in localization on the thiophene units as the LUMO of the calculated trimer has a lower electron density on these units than the LUMO+3 (Figure 4b). Internal conversion from higher excited states of PCPDTBT to the S_1 excited state has been measured by Lanzani et al. using transient absorption spectroscopy and was found to have a time constant of approximately 60 fs when using a pump wavelength of 640 nm[19] and 300 fs when using a pump wavelength of 510 nm, respectively.[20] Here, we found the conversion of S_n electrons formed with a pump wavelength of 400 nm to have a time constant of less than 50 fs. In contrast to this, S_1 electrons have a significantly longer lifetime with an initial decay constant of approximately 1.1 ps (Table 1).

Conclusions

To summarize, we have shown that we can measure binding energies of the ground state as well as excited state in the polymer PCPDTBT by combining an HHG light source with an angle resolved time-of-flight spectrometer. With this set-up, we were able to measure photoelectron spectra following excitation with different pump energies as well as the temporal evolution of these spectra with femtosecond time resolution.

Specifically we measured the fate of the electronic structure when exciting with either 400 or 800 nm. A few hundred femtoseconds after excitation the photoelectron spectra with pump pulses of 400 nm and 800 nm have the same shape suggesting that the systems are in the same excited state at these times. However, directly after excitation the structures are clearly different and by following the immediate temporal evolution of the excitation with 400 nm, we could measure kinetics at timescales

suggesting internal conversion from higher excited states to the first singlet excited state.

To our knowledge, this paper presents the first TRPES study with an XUV source on a conjugated polymer of relevance for organic solar cells. Combining a short pulse X-ray or XUV source with an ARTOF spectrometer opens up many possibilities for further studies of the excited electronic structure of this type of materials. Such studies will enhance the understanding of how they function in solar cells. In the future, we plan to use TRPES for the study of complete donor-acceptor interfaces in organic solar cells, which will allow us to follow the electronic structure during the charge separation process. This will enable the determination of both the magnitude and kinetics of energy losses in specific charge transfer processes.

Supporting information

X-ray photoelectron spectra of PCPDTBT, detailed DFT calculation results, error analysis of TRPES data, details of the kinetic fitting procedure, estimation of surface excitation densities.

Conflict of interest

The authors declare no conflict of interest.

Acknowledgements

We would like to thank Nils Krebs for his help in setting up the first version of a pump-probe setup at HELIOS with an ARTOF and Ruslan Ovsyannikov for his support in operating and trouble-shooting the ARTOF and development of the ARTOF data evaluation software package for Igor Pro. It was possible to design, construct and build HELIOS thanks to financial support from Knut and Alice Wallenberg foundation (KAW), which is gratefully acknowledged. The ARTOF was financed by VINNOVA in Sweden. We also acknowledge the financial support of Swedish Research Council (VR), the European Research Council under the European Union's Seventh Framework Programme (FP7/2007-2013) / ERC grant agreement n° [321319], the Carl Tryggers foundation, the Swedish Energy agency, the Swedish Research Council FORMAS, ÅForsk, additional financial support from KAW and the Göran Gustafsson Foundation.

References:

1 T. M. Clarke and J. R. Durrant, *Chem. Rev.*, 2010, **110**, 6736–67.
2 K. Vandewal, S. Albrecht, E. T. Hoke, K. R. Graham, J. Widmer, J. D. Douglas, M. Schubert, W. R. Mateker, J. T. Bloking, G. F. Burkhard, A. Sellinger, J. M. J. Fréchet, A. Amassian, M. K. Riede, M. D. McGehee, D. Neher and A. Salleo, *Nat. Mater.*, 2014, **13**, 63–8.
3 G. Yu, J. Gao, J. C. Hummelen, F. Wudl and A. J. Heeger, *Science*, 1995, **270**, 1789–1791.
4 J. J. M. Halls, C. A. Walsh, N. C. Greenham, E. A. Marseglia, R. H. Friend, S. C. Moratti and A. B. Holmes, *Nature*, 1995, **376**, 498–500.
5 R. Berera, R. van Grondelle and J. T. M. Kennis, *Photosynth. Res.*, 2009, **101**, 105–118.
6 I. A. Howard and F. Laquai, *Macromol. Chem. Phys*, 2010, **211**, 2063–2070.
7 A. Stolow, *Annu. Rev. Phys. Chem.*, 2003, **54**, 89–119.
8 A. Stolow, A. E. Bragg and D. M. Neumark, *Chem. Rev.*, 2004, **104**, 1719–

1757.
9 G. Wu, P. Hockett and A. Stolow, *Phys. Chem. Chem. Phys.*, 2011, 13, 18447.
10 X.-Y. Zhu, *Annu. Rev. Phys. Chem.*, 2002, **53**, 221–47.
11 M. Weinelt, *J. Phys. Condens. Matter*, 2002, **14**, R1099–R1141.
12 C. Zhou, Z. Ma, Z. Ren, A. M. Wodtke and X. Yang, *Energy Environ. Sci.*, 2012, **5**, 6833.
13 A. McPherson, G. Gibson, H. Jara, U. Johann, T. S. Luk, I. A. McIntyre, K. Boyer and C. K. Rhodes, *J. Opt. Soc. Am. B*, 1987, **4**, 595–601.
14 S. Plogmaker, J. A. Terschlüsen, N. Krebs, M. Svanqvist, J. Forsberg, U. B. Cappel, J.-E. Rubensson, H. Siegbahn and J. Söderström, *Rev. Sci. Instrum.*, 2015, **86**, 123107.
15 S. Plogmaker, Techniques and Application of Electron Spectroscopy Based on Novel X-ray Sources. Uppsala University, 2012.
16 R. Ovsyannikov, P. Karlsson, M. Lundqvist, C. Lupulescu, W. Eberhardt, A. Föhlisch, S. Svensson and N. Mårtensson, *J. Electron Spectros. Relat. Phenomena*, 2013, **191**, 92–103.
17 J. Peet, J. Y. Kim, N. E. Coates, W. L. Ma, D. Moses, A. J. Heeger and G. C. Bazan, *Nat. Mater.*, 2007, **6**, 497–500.
18 D. Mühlbacher, M. Scharber, M. Morana, Z. Zhu, D. Waller, R. Gaudiana and C. Brabec, *Adv. Mater.*, 2006, **18**, 2884–2889.
19 D. Fazzi, G. Grancini, M. Maiuri, D. Brida, G. Cerullo and G. Lanzani, *Phys. Chem. Chem. Phys.*, 2012, **14**, 6367–74.
20 G. Grancini, M. Maiuri, D. Fazzi, A. Petrozza, H.-J. Egelhaaf, D. Brida, G. Cerullo and G. Lanzani, *Nat. Mater.*, 2013, **12**, 29–33.
21 S. Albrecht, W. Schindler, J. Kurpiers, J. Kniepert, J. C. Blakesley, I. Dumsch, S. Allard, K. Fostiropoulos, U. Scherf and D. Neher, *J. Phys. Chem. Lett.*, 2012, **3**, 640–645.
22 T. Clarke, A. Ballantyne, F. Jamieson, C. Brabec, J. Nelson and J. Durrant, *Chem. Commun.*, 2009, 89–91.
23 A. Rao, P. C. Y. Chow, S. Gélinas, C. W. Schlenker, C.-Z. Li, H.-L. Yip, A. K.-Y. Jen, D. S. Ginger and R. H. Friend, *Nature*, 2013, **500**, 435–9.
24 M. Morana, H. Azimi, G. Dennler, H.-J. Egelhaaf, M. Scharber, K. Forberich, J. Hauch, R. Gaudiana, D. Waller, Z. Zhu, K. Hingerl, S. S. van Bavel, J. Loos and C. J. Brabec, *Adv. Funct. Mater.*, 2010, **20**, 1180–1188.
25 U. Aygül, H. Peisert, J. Frisch, A. Vollmer, N. Koch and T. Chassé, *ChemPhysChem*, 2011, **12**, 2345–51.
26 M. J. Frisch, G. W. Trucks, H. B. Schlegel, G. E. Scuseria, M. A. Robb, J. R. Cheeseman, G. Scalmani, V. Barone, B. Mennucci, G. A. Petersson, H. Nakatsuji, M. Caricato, X. Li, H. P. Hratchian, A. F. Izmaylov, J. Bloino, G. Zheng, J. L. Sonnenberg, M. Hada, M. Ehara, K. Toyota, R. Fukuda, J. Hasegawa, M. Ishida, T. Nakajima, Y. Honda, O. Kitao, H. Nakai, T. Vreven, J. A. Montgomery Jr., J. E. Peralta, F. Ogliaro, M. Bearpark, J. J. Heyd, E. Brothers, K. N. Kudin, V. N. Staroverov, R. Kobayashi, J. Normand, K. Raghavachari, A. Rendell, J. C. Burant, S. S. Iyengar, J. Tomasi, M. Cossi, N. Rega, J. M. Millam, M. Klene, J. E. Knox, J. B. Cross, V. Bakken, C. Adamo, J. Jaramillo, R. Gomperts, R. E. Stratmann, O. Yazyev, A. J. Austin, R. Cammi, C. Pomelli, J. W. Ochterski, R. L. Martin, K. Morokuma, V. G. Zakrzewski, G. A. Voth, P. Salvador, J. J. Dannenberg, S. Dapprich, A. D. Daniels, Ö. Farkas, J. B. Foresman, J. V Ortiz, J. Cioslowski and D. J. Fox, *Gaussian Inc Wallingford CT*, 2009, 34, Wallingford CT.

27 D. P. Hagberg, T. Edvinsson, T. Marinado, G. Boschloo, A. Hagfeldt and L. Sun, *Chem. Commun.*, 2006, 2245–7.
28 T. Marinado, D. P. Hagberg, M. Hedlund, T. Edvinsson, E. M. J. Johansson, G. Boschloo, H. Rensmo, T. Brinck, L. Sun and A. Hagfeldt, *Phys. Chem. Chem. Phys.*, 2009, **11**, 133–41.
29 P. K. Nayak, G. Garcia-Belmonte, A. Kahn, J. Bisquert and D. Cahen, *Energy Environ. Sci.*, 2012, **5**, 6022.
30 J. Hwang, A. Wan and A. Kahn, *Mater. Sci. Eng. R Reports*, 2009, **64**, 1–31.
31 C. Risko, M. D. McGehee and J.-L. Brédas, *Chem. Sci.*, 2011, **2**, 1200–1218.
32 T. Leitner, Ultrafast processes in molecules visualized with femtosecond pump-probe photoelectron spectroscopy. Universitätsbibliothek der Technischen Universität Berlin, 2012.
33 F. Etzold, I. A. Howard, N. Forler, D. M. Cho, M. Meister, H. Mangold, J. Shu, M. R. Hansen, K. Müllen and F. Laquai, *J. Am. Chem. Soc.*, 2012, **134**, 10569–83.
34 J. Guo, H. Ohkita, H. Benten and S. Ito, *J. Am. Chem. Soc.*, 2009, **131**, 16869–16880.
35 A. A. Paraecattil, S. Beaupré, M. Leclerc, J.-E. Moser and N. Banerji, *J. Phys. Chem. Lett.*, 2012, **3**, 2952–2958.